Molecular Dynamics of Ethylene Glycol Dimethacrylate Glass Former: Influence of Different Crystallization Pathways

ARTICLE *in* THE JOURNAL OF PHYSICAL CHEMISTRY B · OCTOBER 2009

Impact Factor: 3.3 · DOI: 10.1021/jp903208k · Source: PubMed

Molecular Dynamics of Ethylene Glycol Dimethacrylate Glass Former: Influence of Different Crystallization Pathways

María T. Viciosa,[†] Natália T. Correia,[†] Manuel Salmerón Sánchez,[‡,§,||] José L. Gómez Ribelles,[‡,§,||] and Madalena Dionísio*[,†]

REQUIMTE, Departamento de Química, Faculdade de Ciências e Tecnologia da Universidade Nova de Lisboa, 2829-516 Caparica, Portugal., Centro de Biomateriales e Ingeniería Tisular, Universidad Politécnica de Valencia, Camino de Vera s/n, E-46022 Valencia, Spain, Centro de Investigación Príncipe Felipe, Avda. Autopista del Saler 16, 46013 Valencia, Spain, and CIBER en Bioingeniería, Biomateriales y Nanomedicina, Valencia, Spain

Received: April 7, 2009; Revised Manuscript Received: August 3, 2009

The crystallization induced by different thermal treatments of a low molecular weight glass former, ethylene glycol dimethacrylate (EGDMA), was investigated by dielectric relaxation spectroscopy (DRS) and differential scanning calorimetry (DSC). The fully amorphous material, dielectrically characterized for the first time, exhibits three relaxation processes: the α-relaxation related to dynamic glass transition whose relaxation rate obeys a Vogel−Fulcher−Tamman−Hesse (VFTH) law and two secondary processes (β and γ) with Arrhenius temperature dependence. Therefore, the evaluation of distinct crystallization pathways driven by different thermal histories was accomplished by monitoring the mobility changes in the multiple dielectric relaxation processes. Besides isothermal cold-crystallization, nonisothermal crystallizations coming from both the melt and the glassy states were induced. While an amorphous fraction, characterized by a glass transition, remains subsequent to crystallization from the melt, no α-relaxation is detected after the material undergoes nonisothermal cold-crystallization. In the latter, the secondary relaxations persist with a new process that evolves at low frequencies, designated as α′ that was also detected at advanced crystallization states under isothermal cold-crystallization. Under the depletion of the α-relaxation, the β-process when detected becomes better resolved keeping the same location prior to crystallization leading to a decoupled temperature dependence relative to the α-process.

Introduction

The stability of amorphous and crystalline states and the factors that govern their interconversion are fundamental aspects in pharmaceutical[1−3] and food[4] industries. Molecular mobility and thermal history are determinant factors that kinetically drive the transformation pathways, i.e., the conversion between the amorphous and crystalline forms or between different polymorphic forms, which are determinant in materials preservation.[1,2,5,6] Indeed, significant molecular mobility can persist in the glassy state enabling, for instance, the occurrence of phase transitions such as crystallization.[7−9] In this context, understanding key questions, such as under what conditions an amorphous leads to crystal formation and the relation between temperature and crystallization pathways, is important for stable storage and the shelf life of amorphous pharmaceuticals.

The chemical and physical properties exhibited by fully amorphous, partial and wholly crystalline forms of the same substance, are significantly different, whose knowledge is also important for medical purposes. In the present work, ethylene glycol dimethacrylate (EGDMA), used as a cross-linking agent in dental restorative composites[10,11] and ophthalmic applications,[12,13] is used to explore the different aspects concerning molecular mobility and relationship between thermal treatment and transformation pathways since it is able to both vitrify and crystallize. Indeed, EGDMA belongs to the *n*-ethylene glycol dimethacrylate family that easily circumvents crystallization entering in the supercooled regime and vitrifying upon further cooling. In previous publications by some of us,[14,15] it was shown that *n*-ethylene glycol dimethacrylates, with $2 \leq n \leq 4$, have the onset of calorimetric glass transition, T_g, at 181, 187, and 190 K, respectively for $n = 2$, 3, and 4. Their molecular mobility was investigated by dielectric relaxation spectroscopy, DRS, where besides the α-relaxation process associated with the cooperative character of the molecular motions on approaching the glass transition, two secondary relaxations, β and γ in decreasing order of temperature, were detected due to more localized motions that remain active below T_g. The γ-process that was attributed to dipolar fluctuations within the ethylene glycol group (see scheme in Experimental Section) revealed to be independent of the size of the ethylene glycol moiety for the three members, while the β-relaxation, ascribed to hindered rotations involving COO dipoles, shifts to higher relaxation times with the increase of *n*.[15] One of the questions that we also addressed previously was how the relaxation processes detected in EGDMA will fit in the trend of the other family members; it will be shown that EGDMA is a glass former whose dynamics behavior follows the general behavior of its counterparts.

Due to its high dielectric response and ability to be obtained either as a nearly fully amorphous glass or a nearly fully crystal, depending on the thermal treatment to which it is subjected, EGDMA is a good candidate to study simultaneously the crystallization process and the mobility of the coexistent

* Corresponding author. E-mail: madalena.dionisio@dq.fct.unl.pt.
[†] Faculdade de Ciências e Tecnologia da Universidade Nova de Lisboa.
[‡] Universidad Politécnica de Valencia.
[§] Centro de Investigación Príncipe Felipe.
[||] CIBER BBN.

10.1021/jp903208k CCC: $40.75
Published on Web 10/05/2009

amorphous fraction. In particular, the differences in molecular mobility, investigated by DRS, of the remaining amorphous fraction upon both isothermal and nonisothermal crystallization are evaluated, allowing inferring about the achieved semicrystalline morphology.

This study also intends to be a further contribution in what concerns the influence of crystallization in the α-relaxation of the remaining amorphous fraction of a low molecular weight compound as studied by dielectric relaxation spectroscopy since the major studies involve polymers such as PET,[16,17] PLLA,[18−21] PLLA copolymers,[22] polycarbonate/poly(ε-caprolactone) blends,[23] aliphatic polyesters,[24] and poly(butylene isophthalate).[25] As far as we know, the only known studies that have been published regarding nonpolymeric systems include, after the pioneering works of Massalska-Arodz et al. for isopentylcyanobiphenyl[26] and Dobbertin et al. for a terephthalic acid dipropyl ester,[27] other glass formers such as isooctyloxycyanobiphenyl,[28] sorbitol,[29] triphenyl phosphite,[30] 2-propanol,[31] acetaminophen,[32] and another pharmaceutical drug.[33]

Crystallization progresses in both low molecular weight compounds and semicrystalline polymers by the nucleation and growth of crystals in the amorphous liquid. The segmental dynamics of the amorphous region of semicrystalline polymers close to the crystals or confined by them in small layers has been proved to be different from that of the amorphous liquid, using both relaxation spectroscopy and calorimetric techniques. The presence of a rigid amorphous region situated between crystal lamellae has been used to describe the dynamical behavior close to the crystallite surfaces (α′-relaxation) as observed, for example, in PET,[16,17,34,35] poly(3-hydroxybutyrate),[36] and PLLA.[18,19,37] Although the crystal morphology and crystal growth are different in low molecular weight compounds, under certain conditions a new relaxation process evolves also in these systems upon isothermal crystallization as found, e.g., in sorbitol[29] and in a terephthalic acid dipropyl ester.[27] Dielectric monitoring of some of these low molecular weight materials presents features similar to semicrystalline polymers such as the reduction and broadening of the α-process (e.g., sorbitol,[29] triphenyl phosphite,[30] and 2-propanol[31]). Nevertheless, an invariance of the α-loss peak shape with the progress of crystallization is reported for isooctyloxycyanobiphenyl,[28] acetaminophen,[32] and another pharmaceutical drug.[33]

A detailed dynamical study concerning the time evolution of intensity, location, and form of the α-relaxation of EGDMA upon isothermal cold-crystallization will be further presented.[38]

Experimental Section

Materials. Ethyleneglycol dimethacrylate (EGDMA) with structure: was supplied by Aldrich, cat. nbr. 33,568-1, MW = 198.22, 98% assay, and used as received. The purity of the compound was verified by ^{1}H NMR δ ppm ($CDCl_3$, 400 MHz): 1.93 (6H, CH_3), 4.39 (4H, OCH_2CH_2O), 5.58 (2H, $C{=}CH_2$), 6.11 (2H, $C{=}CH_2$). The NMR spectrum reveals the presence of only dimethacrylate-substituted ethyleneglycol, with no evidence of byproducts.

SCHEME 1: Schematic Representation of the Three Experimental Protocols Described in the Text Used to Follow Cold-Crystallization

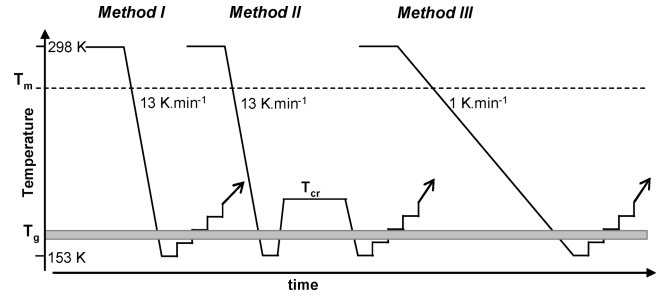

An important reason for choosing this compound is due to its high dielectric strength for the dominating α-process, which can be justified by the large dipole moment 5.3−5.4 D as estimated for the isolated molecule.[39]

Dielectric Relaxation Spectroscopy. Dielectric measurements were carried out using the ALPHA-N impedance analyzer, covering a frequency range from 10^{-1} Hz to 1 MHz. A drop of the EGDMA with two silica spacers 50 μm in thickness was placed between two gold-plated electrodes (diameter 20 mm) of a parallel plate capacitor, BDS 1200. The sample cell was mounted on a cryostat, BDS 1100, and exposed to a heated gas stream being evaporated from a liquid nitrogen Dewar. The temperature control is assured by the Quatro Cryosystem and performed within ± 0.5 K. Novocontrol GmbH supplied all these modules.

The molecular mobility of EGDMA was evaluated in the amorphous and semicrystalline sample after the occurrence of crystallization differently induced.

The fully amorphous state was only studied between 158 and 187 K since cold- crystallization occurred at higher temperatures. Crystallization was induced by three different thermal treatments outlined in Scheme 1.

Method I: Nonisothermal Cold-Crystallization.

Stage (1): The sample was cooled down from 298 to 153 K at 13 K·min^{-1}. As will be shown later, this cooling rate was high enough to avoid crystallization on cooling.

Stage (2): Dielectric measurements were taken isothermally increasing the temperature in different steps from 158 up to 273 K: in the temperature range 158 K ≤ T ≤ 178 K and 233 K ≤ T ≤ 273 K, the dielectric spectra were recorded every 5 K; between 178 and 233 K, the spectra were recorded every 2 or 3 K.

Crystallization occurred at temperatures higher than 187 K. The behavior observed below 187 K corresponds to fully **amorphous** EGDMA.

Method II: Isothermal Cold-Crystallization.

Stage (1): The sample was cooled down from 298 to 153 K at a rate of 13 K·min^{-1}, avoiding crystallization.

Stage (2): It was rapidly heated to the crystallization temperature, T_{cr} (193 or 197 K); several other temperatures were tested, but full results will be reported elsewhere.[38]

Stage (3): At T_{cr}, real-time dielectric measurements were performed by scanning successive frequency sweeps from 1 Hz to 1 MHz every 90 s during 2 h.

Stage (4): The sample was quickly cooled down to 153 K.

Stage (5): Stage (2) of method I.

Method III: Nonisothermal Melt-Crystallization.

Stage (1): The sample was subject to a slow cooling run performed at 1 K·min^{-1} from 298 K down to 153 K.

Stage (2): Stage (2) of method I.

Fresh EGDMA samples were used in each procedure.

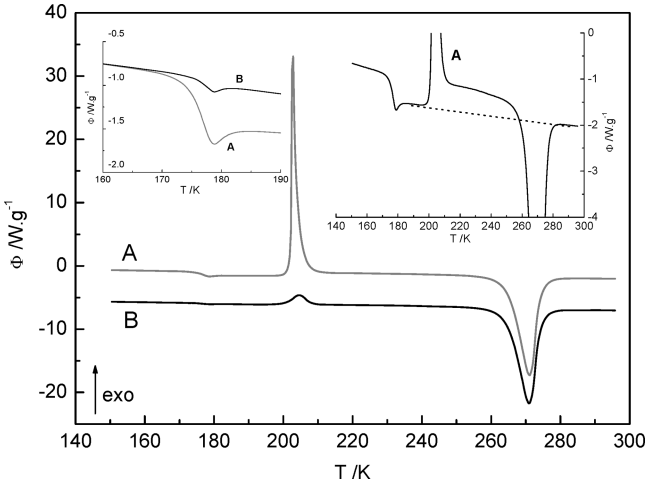

Figure 1. DSC thermograms recorded at heating rate of 10 K·min^{-1} after a previous cooling run at (A) 20 K·min^{-1} and (B) 1 K·min^{-1}. The inset in the left top side is a closeup of the glass transition region for both thermograms A and B where curves were vertically displaced to coincide the initial heat flow; the right-hand inset is a detailed amplified vertical axis of thermogram A.

Data Analysis. To analyze the dielectric response, the model function introduced by Havriliak−Negami was fitted to both imaginary and real components of complex permittivity.[40] Because multiple peaks are observed in the available frequency window, a sum of HN-functions is employed

$$\varepsilon^*(f) = \varepsilon_\infty + \sum_j \frac{\Delta\varepsilon_j}{[1 + (i\omega\tau_{HN})^{\alpha_{HNj}}]^{\beta_{HNj}}} \qquad (1)$$

where j is the index over which the relaxation processes are summed; $\Delta\varepsilon$ is the dielectric strength; τ_{HN} is the characteristic HN relaxation time; and α_{HN} and β_{HN} are fractional parameters ($0 < \alpha_{HN} \leq 1$ and $0 < \alpha_{HN}\beta_{HN} \leq 1$) describing, respectively, the symmetric and asymmetric broadening of the complex dielectric function.[41]

From the estimated values of τ_{HN}, α_{HN}, and β_{HN} fitting parameters, a model-independent relaxation time, τ_{max} ($= 1/2\pi f_{max}$), was determined (see refs 41−43 for details).

Differential Scanning Calorimetry. Differential scanning calorimetry (DSC) was performed using a Pyris 1 apparatus (Perkin-Elmer). The temperature was calibrated by using zinc and indium. The melting heat of indium was used to calibrate the heat flow.

Results

1. Influence of Cooling Rate in Transformation Pathways. ***Differential Scanning Calorimetry.*** EGDMA crystallizes or vitrifies on cooling from the equilibrium liquid depending on the cooling rate. Figure 1 presents DSC thermograms recorded at a heating rate of 10 K·min^{-1} after a previous cooling of, respectively, 20 K·min^{-1} (curve A) and 1 K·min^{-1} (curve B).

The thermogram obtained after the fastest cooling scan (curve A) shows at the lowest temperatures a heat flow jump that is the characteristic glass transition signature. At higher temperatures, around 203 K, an exothermic peak characteristic of a crystallization process emerges. At even higher temperatures, an endothermic peak, with minima a few degrees below 273 K, is observed due to melting. The T_g determined as the temperature of the midpoint of the heat capacity increment in the transition is 175.7 K, and the increment of heat capacity in the transition is $\Delta c_p(T_g) = 114.9$ J·(K·mol)$^{-1}$. The glass transition is quite narrow, covering just $\Delta T_g = 3.5$ K. The onset of the crystallization peak is at 202.0 K, and the maximum of the crystallization exotherm is at 202.7 K. Melting starts at 264.8 K, and the maximum of the endotherm is at 271.2 K. It is interesting to note the step in the measured heat flow in the crystallization transition (see the inset in the right side of Figure 1) that indicates the difference between the heat capacity of the liquid (at temperatures in the interval between the glass transition and the onset of crystallization) and the solid phase (at temperatures above the exotherm). A straight line has been drawn joining the liquid states just above the glass transition and just above melting showing that the thermogram in the temperature interval when the sample is in the solid phase is above this line. The difference between the heat capacity of the solid and the liquid seems to be in the order of magnitude of the heat capacity increment in the glass transition as it should since the heat capacity of the glass should not be very different from that of the crystal. The area measured in the thermogram from 188 K a temperature just above the glass transition (188 K) to 293 K, taking the straight dashed line of Figure 1 as baseline for integration, is slightly endothermic, around 0.8 ± 0.4 kJ·mol^{-1}, while the area of the melting peak is 20.2 ± 0.6 kJ·mol^{-1}. This means that after cooling at 20 K·min^{-1} a few percent of the mass of the sample can be in the crystalline state before the glass transition; thus, the heat capacity increment determined from the thermogram can be slightly underestimated.

The discontinuity in the heat flow due to the glass transition is hardly seen in the DSC thermogram recorded after a previous cooling at 1 K·min^{-1} (curve B in Figure 1), as a consequence of crystallization that occurred at this quite slow cooling rate; the inset at the left top of Figure 1 enhances the respective heat flow step. Thus, the sample at the beginning of the heating scan, at 133 K, is in a semicrystalline state. The melting peak further detected exactly matches that recorded after cooling at 20 K·min^{-1}.

EGDMA is thus a material that exhibits a significant shift (∼60°) between the temperature regions where crystallization and melting occur.

Dielectric Relaxation Spectroscopy. The influence of cooling rate was also evaluated by DRS. Figure 2 presents the isochronal plots of both ε' and ε'' at 1 kHz collected in ramp experiments during the descending step to 153 K of crystallization methods **I** (open circles) and **III** (open triangles) (see Experimental Section); the corresponding heating runs (isothermal data acquisition) are represented in filled symbols.

On cooling at 13 K·min^{-1} (procedure **I**), the trace of the real part of the complex permittivity shows a marked fall just before 193 K indicating the transformation, at the measuring frequency, from the supercooled liquid to the glass, which, in the ε'' trace, corresponds to an intense peak, i.e., the relaxation process associated to the glass transition. On the other hand, both ε' and ε'' traces concerning the cooling at 1 K·min^{-1} (procedure **III**) show a sharp decrease just below 233 K due to crystallization. Although strongly depleted, there still exists a relaxational contribution around 193 K due to the remaining amorphous fraction that shows up at lower temperatures in ε'', similarly to the previous sample (procedure **I**) meaning that the sample did not reach full crystallization, being in a semicrystalline state.

The absence of discontinuity in both ε' and ε'' traces upon cooling at a higher rate (procedure **I**) until the region where the α-relaxation evolves leads us to conclude that EGDMA crystallization was circumvented. The rise observed in ε' with

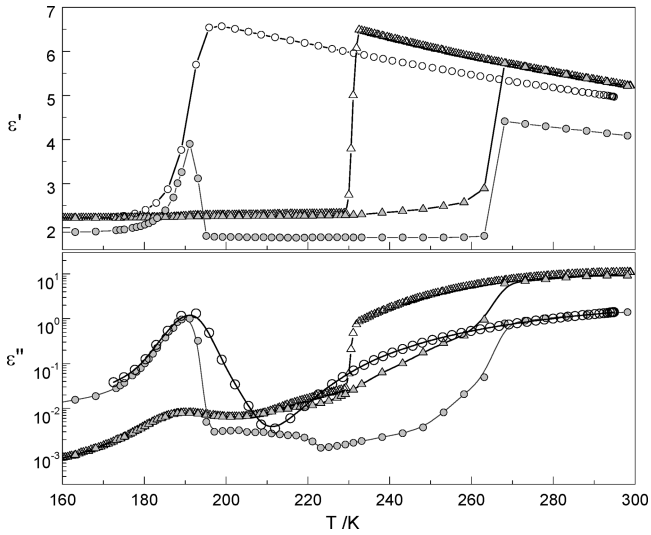

Figure 2. Isochronal plots of both real, ε', and imaginary, ε'', parts of the complex permittivity at 1 kHz collected in a cooling ramp from 298 to 153 K: at 13 K·min^{-1}, open circles; and at 1 K·min^{-1}, open triangles. The sharp drop around 233 K in the ε' trace obtained at 1 K·min^{-1} (triangles) indicates that crystallization occurred which is avoided when cooling is carried out at 13 K·min^{-1}. Filled gray symbols represent the ε' and ε'' traces taken from isothermal data acquisition on heating after each cooling ramp.

the temperature decrease is caused by the expected increase of the dielectric strength and can be quantified according to the Fröhlich−Kirkwood equation[41,44]

$$\varepsilon_s - \varepsilon_\infty = \frac{\mu_0^2 g \frac{N}{V} \varepsilon_s (\varepsilon_\infty + 2)^2}{3\varepsilon_0 k_B T 3(2\varepsilon_s + \varepsilon_\infty)} \quad (2)$$

where μ_0 is the dipolar moment of the isolated dipole; g takes into account the dipole−dipole correlation (for parallel or antiparallel correlations between neighboring dipoles, $g > 1$ or $0 < g < 1$, respectively, while for a random orientation distribution of dipoles, $g = 1$); ε_s and ε_∞ are the limits of the real part of the dielectric permittivity at low and high frequencies, respectively, the latter being approximately the permittivity of the glass;[26] ε_0 is the vacuum permittivity; N/V is the number of dipoles per unit of volume; and k_B is the Boltzmann constant. Thus, from eq 2 the dielectric strength ($\Delta\varepsilon = \varepsilon_s - \varepsilon_\infty$) is proportional to $\mu_0^2 g/9\varepsilon_0 k_B T$. If it is assumed that g is constant, an increase in $\Delta\varepsilon$ from 293 to 198 K of 32% is predicted. The observed raise is 30% (from 5.0 to 6.5), close to the predicted value, making it reasonable to assume that no dipolar moment is lost due to immobilization that would occur if crystallization had taken place. It should be pointed out that in replicate measurements it was found that crystallization can be avoided under cooling rates down to 6 K·min^{-1}.

Upon further heating, the fully amorphous sample undergoes cold-crystallization[45,46] which is visible in the plot just above 193 K by an abrupt decrease in both ε' and ε'' (filled circles). The jump in both real and imaginary parts to higher values observed around 263 K is due to the melting of the crystalline fraction thus formed.

The melting of the semicrystalline sample obtained by method **III** (filled triangles) occurs in the same temperature region where the cold-crystallized sample melts (263 K), which is very close to the onset of the melting endotherm peak detected in DSC heating thermograms (264.8 K).

Mobility in the Amorphous State. According to the dielectric monitoring, crystallization was avoided in the cooling run carried out at 13 K·min^{-1}. Thus, the material is in the glassy state at the beginning of the subsequent heating stage, where dielectric loss spectra were taken isothermally (stage 2 of method **I** in Experimental Section). The ε'' isotherms between 173 and 195 K are shown in Figure 3, and three representative isotherms taken at the lowest temperatures are shown in the inset.

The spectra show a strong relaxation process associated with the dynamic glass transition, an α-relaxation that dominates at the lowest temperatures. The intensity of this main relaxation is comparable to the magnitude of the same process in the other members of the series.[15]

The fully amorphous state is only observed for $T \leq 187$ K. For higher temperatures, the strength of the α-process starts decreasing due to cold-crystallization and is reduced essentially to zero at 198 K. From 178 to 197 K, the main process is well-defined allowing the HN function (eq 1) to fit the experimental data (fitting parameters in Table 1). The estimated shape parameters are in very close agreement with those of its counterparts whose values were also included in Table 1, allowing constructing a master curve (not shown).

At the lowest temperatures, three individual HN functions were necessary to describe the complete spectrum: the main relaxation process and the two secondary processes, β and γ (see Introduction). Due to the proximity of the main α-relaxation process, only few spectra allowed the β-relaxation to be resolved in the fitting procedure before the onset of crystallization. The γ-relaxation is also difficult to define since it always arises merged under the more intense β-relaxation; however, it was always considered in the fits. The estimated α_{HN} and β_{HN} values are (0.50, 0.94) and (0.41, 0.44), respectively, for the β- and γ-processes.

The temperature dependences of the model-independent relaxation times, τ_{max}, are presented in the relaxation map shown in Figure 4 that also includes the activation plots of the other n-ethylene glycol dimethacrylates ($2 \leq n \leq 4$). Concerning the α-relaxation of EGDMA, no discontinuity is found in its temperature dependence when comparing τ_{max} taken from the lowest temperatures at which the sample is in the wholly amorphous state (black circles) and at higher temperatures where τ_{max} was estimated from loss curves strongly depleted due to crystallization (open circles). Thus, we believe that the reported dynamical behavior was meaningfully affected by crystallization being not far from the one that would be found for the fully amorphous material.

The dynamical behavior of the α-process is predominantly non-Arrhenian contrarily to the glassy state dynamics where relaxation times obey a linear temperature dependence. The curvature of the characteristics relaxation times, τ, in function of temperature reciprocal is often described by the empirical Vogel−Fulcher−Tamman−Hesse (VFTH) equation[47−49]

$$\tau(T) = \tau_\infty \exp\left(\frac{B}{T - T_0}\right) \quad (3)$$

where τ_∞, B, and T_0, the so-called Vogel temperature, are empirical parameters characteristic of the material. The parameters obtained from the VFTH fit of the plot of $-\ln \tau_{max,\alpha}$ vs the reciprocal of temperature are listed in Table 1, which allow us to estimate the glass transition temperature at $\tau = 100$ s,[50] as 171.4 K.

Commonly, the degree of deviation from Arrhenius-type temperature dependence near T_g provides a useful classification

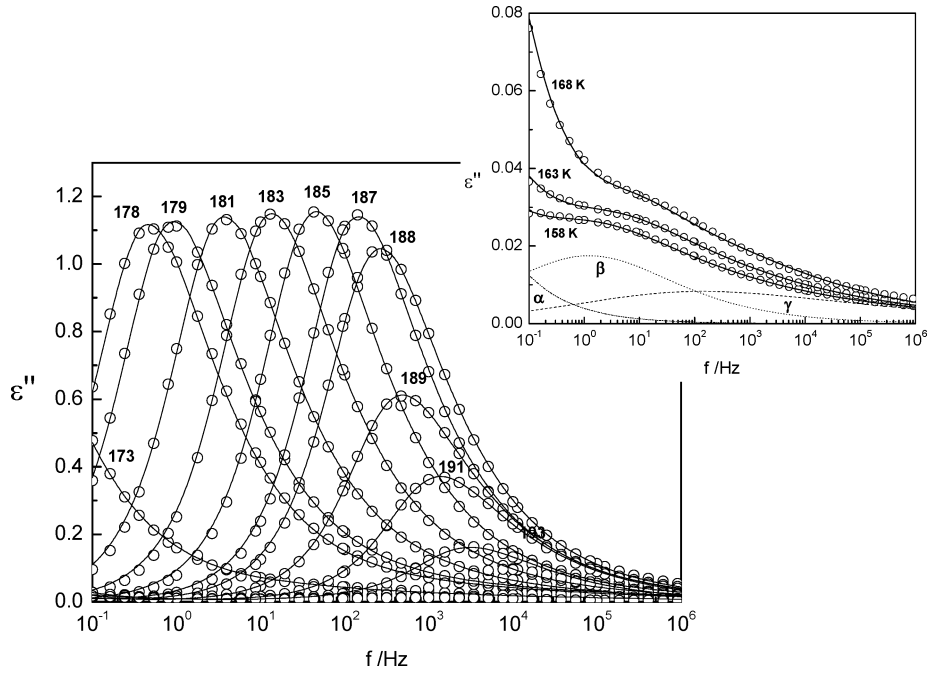

Figure 3. Isothermal dielectric loss spectra obtained between 173 and 195 K, after a cooling ramp carried out at 13 K·min^{-1} from 298 to 153 K; in the inset, the isotherms taken below T_g evidence the two secondary processes. All solid lines are the overall HN fit to the experimental data considering a sum of HN individual functions that are exemplified as dashed lines in the inset for the isotherm at 158 K.

TABLE 1: Shape Parameters (α_{HN}, β_{HN}) Obtained from the HN Fitting to the Main Relaxation Process of EGDMA[a]

	EGDMA	DEGDMA[b]	TrEGDMA[c]	TeEGDMA[b]
α_{HN}	0.94 ± 0.02	0.92 ± 0.04	0.95 ± 0.03	0.94 ± 0.03
β_{HN}	0.51 ± 0.03	0.52 ± 0.03	0.46 ± 0.03	0.46 ± 0.05
τ_∞/s	(5 ± 5) × 10^{-21}	(7 ± 4) × 10^{-17}	(3 ± 1) × 10^{-16}	(7 ± 4) × 10^{-15}
B/K	2820 ± 586	1695 ± 97	1520 ± 52	1251 ± 87
T_0/K	117 ± 7	139 ± 2	147 ± 1	154 ± 2
T_g (τ =100 s)/K	171.4	179.6	184.9	187.9
T_g(DSC)/K	175.7	181	187	190
m	70	80	85	90
E_{Tg}^{app}/kJ·mol^{-1}[d]	229	276	303	325

[a] VFTH parameters (eq 3), glass transition temperature, T_g, estimated at τ = 100 s, T_g calorimetric, T_g(DSC), obtained at a heating rate of 10 K·min^{-1}, fragility index, m (eq 5), and apparent activation energy at T_g, E_{Tg}^{app}. The respective data for the other n-ethylene glycol dimethacrylates are included. [b] Data from ref 15. [c] Data from ref 14. [d] The apparent activation energy, $E^{app} = R\partial \ln \tau \partial 1/T$, was determined from the VFTH parameters, at T_g, as $E_{Tg}^{app} = RB(1 - T_0/T_g)^2$.

of glass formers.[51,52] A quantitative measure of the fragility can be obtained from the steepness index m according the following equation

$$m = \left.\frac{\mathrm{d}\log_{10}\tau(T)}{\mathrm{d}(T_g/T)}\right|_{T=T_g} \quad (4)$$

Using the VFTH expression (eq 3) together with eq 4, m can be estimated as

$$m = \frac{BT_g}{\ln 10(T_g - T_0)^2} \quad (5)$$

which, for EGDMA, taking the B and T_0 values determined for the VFTH fit to the α-relaxation (Table 1), gives a fragility index of m = 70 in line with the behavior of the other members of the series, where m increases with the number of ethylene glycol units.

For the γ-relaxation, the pre-exponential, τ_∞, and activation energy, E_a, values estimated from the Arrhenius temperature dependence, $\tau(T) = \tau_\infty \exp(E_a/RT)$, are, respectively, (1.2 ± 0.9) × 10^{-16} s and 39 ± 3 kJ·mol^{-1}. Activation parameters for the β-process will be given in the next section.

Mobility after Nonisothermal Cold-Crystallization (I). The 3D plot shown in Figure 5 evidences the relaxation processes found after the nonisothermal cold-crystallization. Above 197 K, the α-process extinguishes allowing the position and shape of the β-relaxation to be defined unequivocally. The latter becomes narrower as compared to the amorphous state (α_{HN} increases from 0.50 to 0.60−0.80). The respective relaxation times temperature dependence (see Figure 4) closely follows the behavior found in the amorphous state. The temperature dependence taking into account the two sets of data, before (filled black circles) and after (open circles) crystallization, shows the linear behavior represented in Figure 4, from which a pre-exponential factor of (2 ± 1) × 10^{-14} s and an activation energy of 38.5 ± 0.5 kJ·mol^{-1} were obtained.

The γ-relaxation, after crystallization, seems to be present in the high frequency side of the spectra; however, no reliable location of its maximum can be provided, which is the reason why no activation parameters are given.

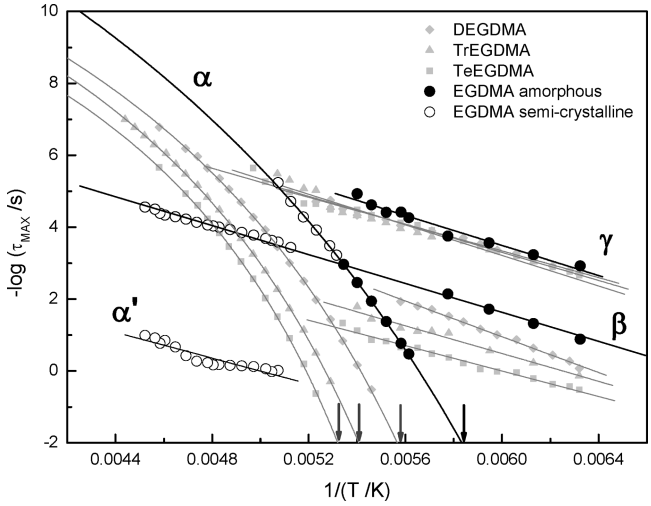

Figure 4. Relaxation map for amorphous EGDMA (filled circles), between 173 and 187 K, and semicrystalline EGDMA (open circles; for temperatures higher than 187 K), obtained after a cooling run at 13 K·min^{-1} from 298 down to 153 K (method **I**). For comparison purposes, the activation data of the other *n*-ethylene glycol dimethacrylates studied by us, DEGDMA,[15] TrEGDMA,[14] and TeEGDMA,[15] are included as gray symbols. The arrows indicate the respective glass transition temperatures, T_g, at $\tau = 100$ s. Solid lines are the respective Arrhenius and VFTH fits; in the latter, since the plot is $\log_{10} \tau$, the estimated *B* parameter was divided by ln 10.

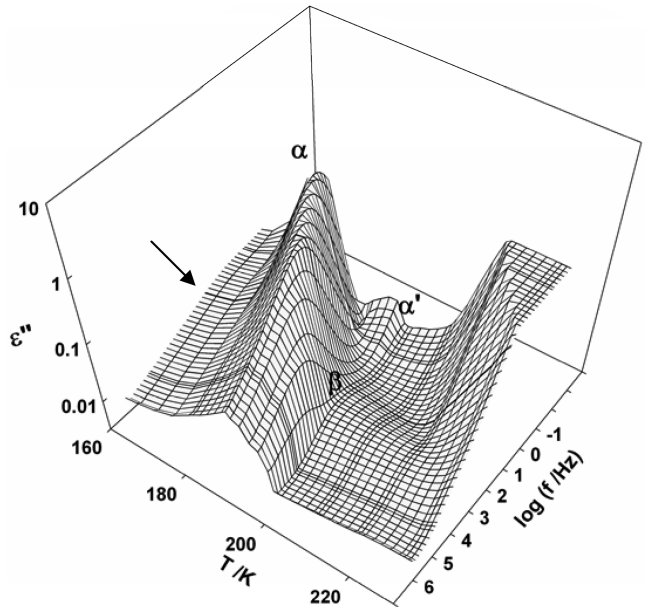

Figure 5. Three-dimensional plot of the isothermal dielectric loss spectra obtained between 173 and 195 K, after a cooling ramp carried out at 13 K·min^{-1} from 298 to 153 K, evidencing the relaxations remaining after cold-crystallization; the arrow indicates the position of the β-process in the glassy state.

At these advanced crystallization degrees, another process evolves at the lowest frequencies, designated as α′ (see Figure 5). The temperature dependence of its relaxation times is included in Figure 4 being nearly Arrhenian with activation parameters: $\tau_\infty = (1.12 \pm 0.08) \times 10^{-12}$ s and $E_a = 46 \pm 4$ kJ·mol^{-1}. This process will be further discussed.

Monitoring in Real Time the Mobility during Isothermal Cold-Crystallization. Figure 6 shows the real time evolution of the dielectric loss during the isothermal cold-crystallization process for (a) 193 K and (b) 197 K, in the frequency range from 0.7 to 10^5 Hz (see method **II** in the Experimental Section). Above this frequency, an increase in ε'' is observed with no physical meaning due to the inaccuracy of measurements at so low ε'' values; therefore, these data are omitted in all spectra.

As a first observation, the decrease of the intensity of the α-relaxation while crystallization progresses is obvious, the extinction occurring faster at the highest temperature (197 K). In this case, the β-relaxation also disappears. Differently, when crystallization is carried out at 193 K, the β-relaxation becomes resolved from the α-process, while the latter becomes extinct. In both cases, at advanced states of crystallization, another relaxation process evolves in the low-frequency flank of the α-peak, designated α′ as before; this process is better seen in Figure 6b.

A sum of HN functions (eq 1) was fitted to the dielectric data collected during crystallization considering the following relaxations: (i) the α-relaxation, which is the major contribution in the first stages of the crystallization process, (ii) the γ-relaxation, located in the high frequency side of the α-peak, (iii) the α′-process that only becomes significant later on, and (iv) the β-process for crystallization monitored at 193 K that turns out to be important when the α-relaxation is strongly depleted. The inset at intermediate crystallization states (see legend) illustrates the individual relaxations considered for each T_{cr}.

The parameters of the individual functions used to fit the loss peaks at each T_{cr} are summarized in Table 2. From the fit of dielectric spectra, it was further deduced that the α-peak does not present any significant changes either in position or in shape. At the end of the 2 h of crystallization, different final states were attained at each T_{cr} exhibiting different relaxation processes. Concerning the condition attained after crystallization at 197 K, in spite of its very low dielectric response, the low frequency flank denotes the presence of the highly constrained α′-relaxation. This process is significantly shifted to lower frequencies when compared with the position of the absent α bulk-like process; the γ-relaxation still contributes in the high frequency region. The major observation relative to the final state achieved after crystallization at 193 K is the presence of the β-process that is still detected in the latter.

Mobility after Isothermal Cold-Crystallization (II). To investigate the relaxation processes that persist after isothermal cold-crystallization, stages 4 and 5 of method **II** were followed.

Figure 7 shows the dielectric response measured after the sample being crystallized isothermally at 197 K.

At the lowest temperatures (gray circles), the remaining γ- and α′-processes are difficult to detect in the isotherms, but the latter is clearly visible as a small peak in the isochronal representation (inset of Figure 7). The spectra do not change significantly with temperature up to 213 K. However, from 213 to 223 K, ε'' suddenly increases at low frequencies due to the appearance of conductivity followed by an unexpected decrease as revealed by an abrupt drop in the inset. This is due to further crystallization. The process that emerges at 233 K is probably a MWS effect due to interfacial polarization built up in the interphases between different crystalline morphologies. Above 263 K, the conductivity abruptly increases due to the melting (clearly visible in the inset).

Figure 8 presents, in the temperature range from 158 to 225 K, the relaxation spectra of the sample previously cold-crystallized at 193 K. The α′-, β-, and γ-relaxation processes that remained after isothermal crystallization are observable, the

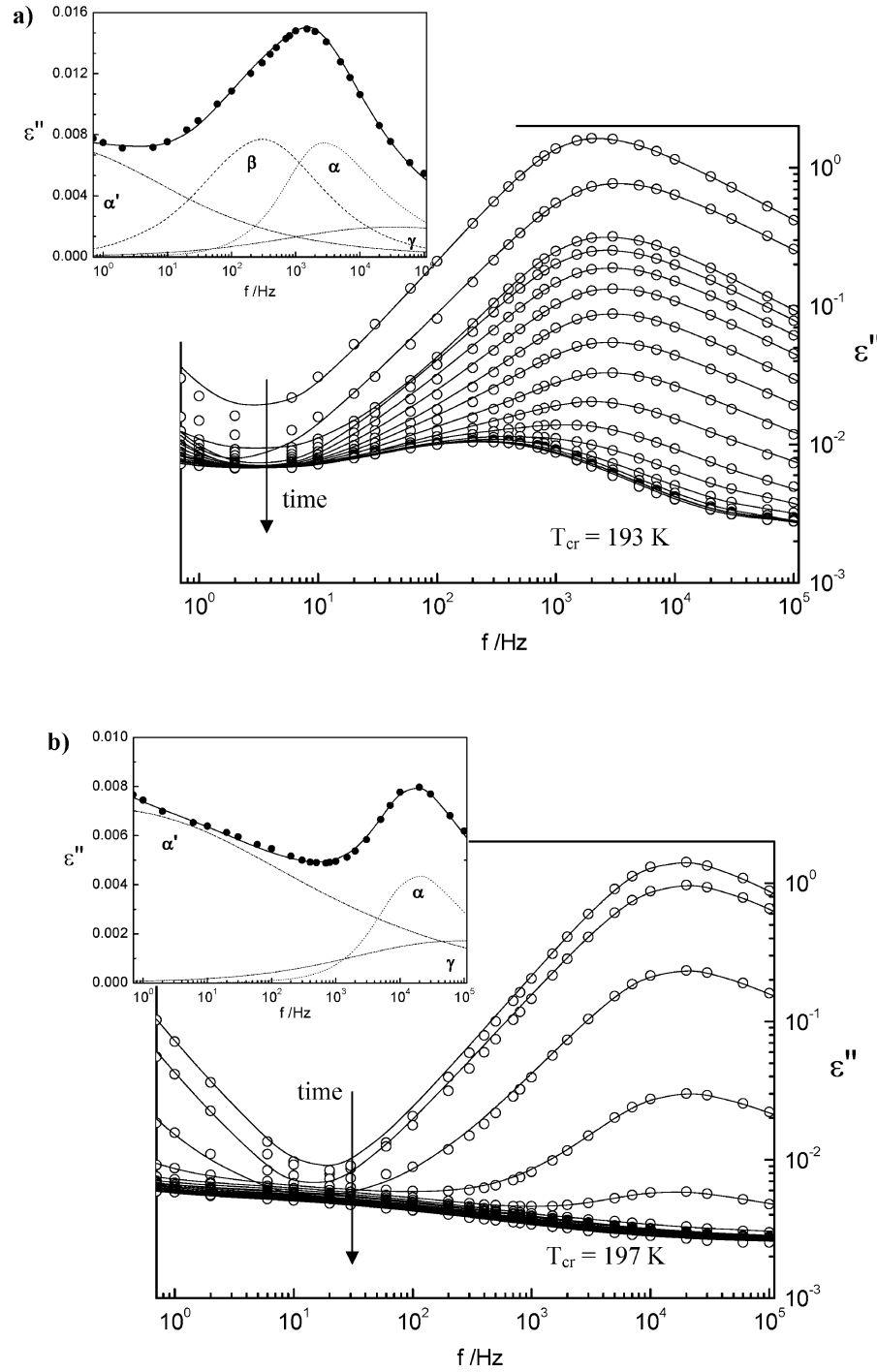

Figure 6. Real time evolution of the dielectric loss collected every six minutes during the isothermal cold-crystallization process over 2 h at (a) 193 K and (b) 197 K. Solid lines are the overall fitting curves, taking into account a sum of three HN individual functions, depicted in the inset (dashed and dotted lines) at intermediate crystallization states (a) 58.5 min and (b) 22.5 min.

TABLE 2: Shape Parameters, α_{HN} and β_{HN}, and Relaxation Time, τ_{HN}, of the Individual Functions Used to Fit the Loss Peaks during Real Time Isothermal Crystallization at Each Crystallization Temperature T_{cr} = 193 K and T_{cr} = 197 K[a]

	α′	β	α	γ
α_{HN} (193 K/197 K)	0.40/0.23	0.63/—[b]	0.94 ± 0.01	0.42/0.42
β_{HN} (193 K/197 K)	0.76/1.00	1.00/—[b]	0.50 ± 0.02	0.44/0.44
τ_{HN}/s (193 K/197 K)	1.2/0.4	5.5×10^{-4}/—[b]	1.1×10^{-4}/1.5×10^{-5}	3.1×10^{-5}/1.2×10^{-5}

[a] All the parameter values presented in the table were kept fixed during fitting with the exception of those affected by uncertainties. [b] This process was not considered in the overall fit since at 197 K EGDMA crystallizes without evidence of the β-process.

β-relaxation being the more prominent. It should be pointed out that in quadruplicate measurements where isothermal cold-crystallization was carried out at 193 K the β-relaxation was observed in the final state three times, while in one of the experiments only the α′-process remains (data reported elsewhere[38]). Three HN functions were considered in the data

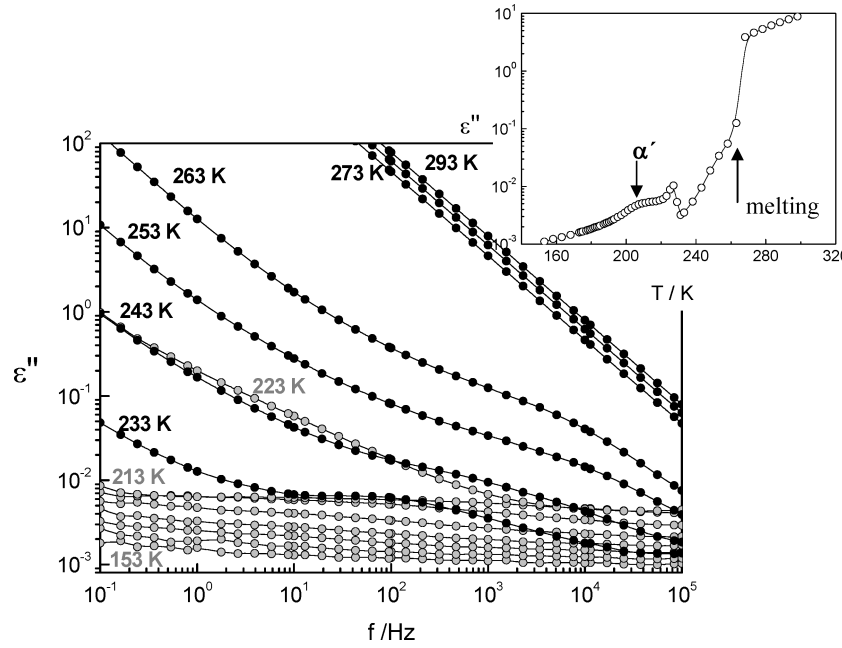

Figure 7. Dielectric loss spectra collected isothermally between 153 and 293 K (here shown in steps of 10 K) after 2 h of isothermal cold-crystallization at 197 K (method **II**). Solid lines are guides for the eyes. The inset shows the corresponding isochronal plot at 1 kHz.

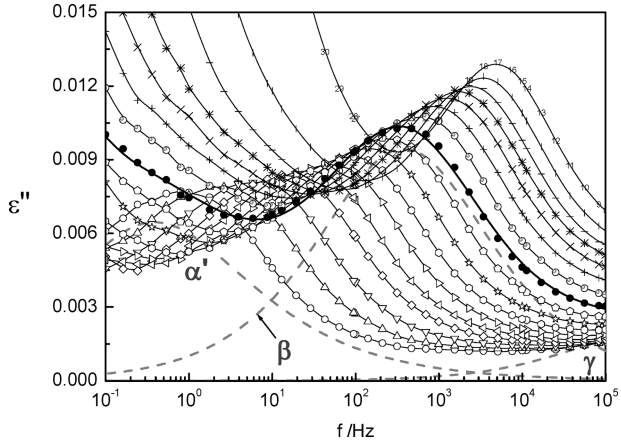

Figure 8. Dielectric loss spectra collected isothermally after 2 h of isothermal cold-crystallization at 193 K for temperatures between 158 and 173 K every 5 K and from 177 to 225 K in steps of 4 K (method **II**). The solid lines are guides to the eyes except for the isotherm at 197 K (filled symbols) for which the solid line represents the overall fit corresponding to a sum of three individual HN functions (gray dashed lines).

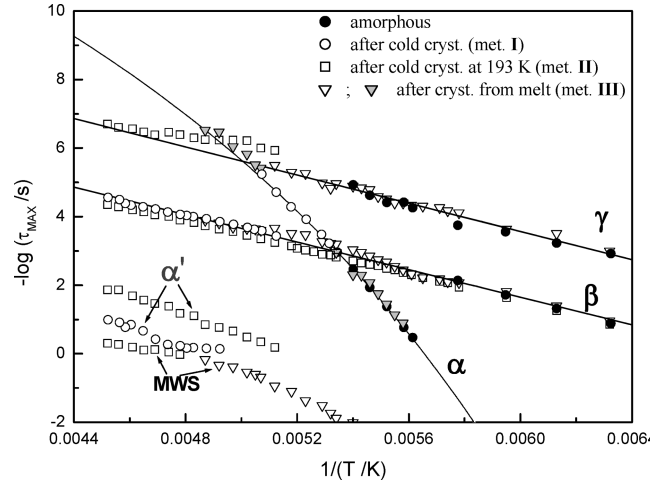

Figure 9. Relaxation map for all detected processes in EGDMA after being previously submitted to the different thermal treatments tested (for more details, see Experimental Section). Solid lines are the Arrhenius and VFTH fits of the relaxations found in amorphous EGDMA.

TABLE 3: Shape Parameters Obtained From the HN Fitting Procedure and Activation Values for the Relaxations Detected after Isothermal Cold-Crystallization at 193 K

	α'	β	γ
α_{HN}	0.61 ± 0.02	0.59 ± 0.05	0.43 ± 0.04
β_{HN}	0.767 ± 0.005	1.00 ± 0.00	0.42 ± 0.02
E_a/kJ·mol^{-1}	56 ± 1	37.7 ± 0.3	$-^a$
τ_∞/s	$(8 \pm 4) \times 10^{-16}$	$(4.8 \pm 0.8) \times 10^{-14}$	$-^a$

[a] The temperature dependence of the relaxation times nearly follows the linear behavior found in the amorphous material (data provided in the text).

treatment, which are illustrated in Figure 8 for the spectrum collected at 197 K; the solid line is the overall fit (see fitting parameters in Table 3).

The temperature dependence of the relaxation times of the different processes is plotted in Figure 9 (activation parameters in Table 3). Figure 9 also presents the relaxation processes observed in the amorphous material for comparison purposes.

The α'-relaxation is accompanied by a fourth process in its low frequency side ascribed to interfacial polarization or Maxwell−Wagner−Sillars (MWS) confirmed by an increase in the real part of the complex permittivity (not shown). The temperature dependence of τ_{MWS} is included in Figure 9 (open squares).

Mobility after Nonisothermal Melt-Crystallization (III). As explained before, EGDMA was subjected to nonisothermal crystallization coming from the melt (see Experimental Section).

An interesting observation is that EGDMA does not undergo significant further crystallization in the heating run: remember Figure 2 where there is superposition below 233 K of both backward scan (open triangles) which corresponds to the cooling ramp measurements and the forward run (filled triangles) that concerns isothermal data acquisition upon heating.

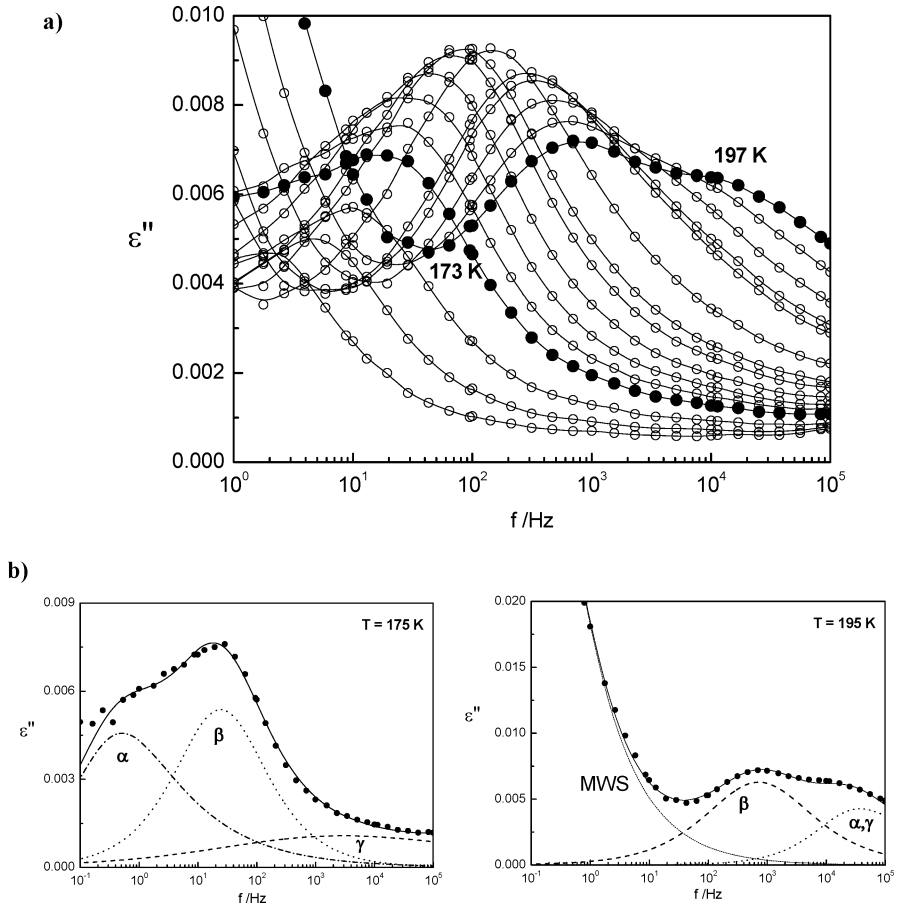

Figure 10. (a) Dielectric loss spectra obtained after crystallization from the melt (at a cooling rate of 1 K·min^{-1}; method **III**) for temperatures between 158 and 173 K, in steps of 5 K, and from 173 to 197 K, in steps of 2 K. (b) Isotherms taken at 175 and 195 K where the solid lines are the overall fit to data using a sum of HN individual functions as exemplified by the dashed and dotted lines.

Figure 10a presents some representative loss curves collected between 158 and 197 K of EGDMA previously crystallized from the melt.

The spectra are dominated by a sharp although low intense process that shows up at the very beginning of measurements, far below the glass transition temperature ($T_g \approx 171$ K). Thus it is ascribed to the β-relaxation, and the γ-relaxation is located in its high frequency side that, in spite of its low intensity, is now more visible than in the fully amorphous sample. The β-peak remains clearly visible in the temperature range shown, although influenced by the α-relaxation from temperatures near below and above T_g. To clarify this, a detailed analysis of the spectra is now provided with the help of Figure 10b which depicts at 175 and 195 K the individual HN functions considered to obtain the overall fit.

At 175 K, the α-process emerges in the low frequency side of the β-relaxation, becoming submerged at 183 K. It overpasses the β-process at 195 K (Figure 10b) swelling the weak γ-relaxation. Its temperature dependence, included in Figure 9 as filled triangles, superimposes that of the α-relaxation found in the amorphous state obeying the same VFTH law.

The strong increase of ε'' at the lowest frequencies shown in Figure 9b is compatible with an interfacial polarization build up in the interface of crystalline/amorphous fractions, i.e., a Maxwell−Wagner−Sillars effect (MWS), confirmed by an increase in the real part of the complex permittivity (not shown).

The activation plots of all detected processes are included in the relaxation map shown in Figure 9, being evident that the α-, β-, and γ-processes of this semicrystalline specimen follow the behavior found for amorphous EGDMA. No α′-process was detected in this sample.

Discussion

Ramp experiments carried out at different cooling rates by either DSC or DRS proved that the glass-former EGDMA can be obtained with different degrees of crystallinity, the slower rates promoting a higher crystallization, as expected.

From calorimetric results, it was concluded that even at a relatively high cooling rate of 20 K·min^{-1} always some degree of crystallization is observed. On the other hand, DRS measurements evidence that at cooling rates in the range from 13 to 6 K·min^{-1} a fully amorphous material is obtained. Thus, the transformation pathway can also be critically dependent on the sample geometry. Although in both techniques the amount of sample is relatively small (around 10 μL), the different way the liquid allocates in each sample holder could be in the origin of different transformations even under similar thermal histories. On the other hand, a fully crystalline material could not be obtained by slow cooling experiments either in DRS or in DSC. Nevertheless, DRS revealed that highly crystalline materials were obtained as evaluated by the depletion of the dielectric strength of the remaining processes that in all semicrystalline specimens investigated is much less than 1% of the original magnitude of the main α-relaxation.

Before an overall discussion, the summary of the dynamic scenario found after each thermal treatment is now provided.

Amorphous State. Three relaxation processes were detected in the amorphous state: the main α-relaxation and two β- and

TABLE 4: Summary of the Detected Processes after Different Thermal Treatments

thermal treatment		detected process				
		γ	β	α	α'	MWS
cooling to 153 at 13 K·min^{-1}; 153 K ≤ T ≤ 187 K (amorphous)		yes (ill-defined)	yes (ill-defined)	yes (strong)	no	no
after non-isothermal cold-crystallization (met. **I**) for T ≥ 198 K		yes	yes (well-defined)	no	yes	—[a]
after isothermal cold-crystallization (met. **II**)	T_{cr} = 193 K	yes	yes[b] (well-defined)	no	yes	yes
	T_{cr} = 197 K	yes (very weak)	no	no	yes	no until 213 K[c]
after crystallization from melt (at cooling rate of 1 K·min^{-1}; met. **III**)		yes	yes	yes (weak)	no	yes

[a] No reliable fitting was possible for this process. [b] The β-process was detected in the isotherms measured after method **II** in three of quadruplicate measurements, while in one the α' was the only remaining process. [c] A particular behavior was observed in this sample for temperatures higher than 223 K; in this new condition, the material exhibits MWS effect.

γ-secondary processes. The dynamical behavior follows, in general, the tendency observed in EGDMA counterparts, namely: (i) the T_g value, detected calorimetrically and estimated from dielectric data, is the lowest obtained for the *n*-ethylene glycol dimethacrylates previously studied (with *n* going from 2 to 4), confirming that the glass transition temperature decreases with the number of ethylene glycol units, (ii) the temperature dependence of the secondary β-relaxation shifts to lower relaxation times with the decrease of the ethylene glycol group size, and (iii) the γ-process temperature and frequency location is independent of *n*. The γ-peak was assigned to dipolar motions within the ethylene glycol moiety, as mentioned in the Introduction, being of very low intensity in EGDMA while comparing to the other members of the series, as expected since it only contains one ethylene glycol group.

The departure from Arrhenian behavior of the α-relaxation is much less pronounced in EGDMA compared with its counterparts as confirmed by the lower fragility index, *m*. Both *m* and the apparent activation energy at T_g (Table 1) decrease with the decrease of glass transition temperature, which indicates that some correlation should exist between the different properties. Indeed, Qin and McKenna[53] proposed a roughly linear relationship between dynamic fragility and the glass transition temperature and their apparent activation energy, E_a^{app} at T_g, with T_g[2] by analyzing data concerning a variety of glass-former systems. For all ethylene glycol dimethacrylates studied by some of us, the predicted correlation obeys E_{Tg}^{app} (kJ·mol^{-1}) = $0.018T_g^2$(K) − 305 with a correlation factor of 0.98 where the T_g values used were those estimated from dielectric data.

Mobility after Nonisothermal Cold-Crystallization. During nonisothermal cold-crystallization, the α-process goes progressively to extinction. The respective shape parameters associated to the isotherms where it is still detected, although with decreasing intensity, stay almost unchanged. After crystallization, the main α-process vanishes, and the secondary β- and γ-processes remain together with a new hindered process (α'). The β-relaxation becomes narrower and much better resolved. The narrowing is associated to a more restricted distribution of relaxation times probably caused by a greater homogeneity of surrounding media. Its linear temperature dependence follows the behavior observed in the glassy state crossing the trace of the α-relaxation of the bulk amorphous fraction.

Mobility under and after Isothermal Cold-Crystallization. Upon isothermal cold-crystallization, the behavior is strongly temperature dependent. At 197 K the α-relaxation rapidly depletes and the same happens with the β-process. On the other side, at 193 K, the α-peak extinguishes, whereas the β-relaxation remains although significantly reduced. The latter never becomes extinct even after further heating. At both crystallization temperatures, the evolution of the α-process occurs with no significant changes either in position or in shape. At relatively high crystallization states, a new relaxation, the α'-process, evolves.

Both β- and α'-processes were characterized in the subsequent measurements performed after the accomplishment of isothermal crystallization at 193 K. The temperature dependence of the α'-process exhibits a slope nearly identical to that found for the corresponding process observed after nonisothermal crystallization.

In regard to the β-relaxation, its detection after the vanishing of the main α-process allowed us to investigate its temperature dependence over the entire temperature range. Its trace in the relaxation map obeys the extrapolation of the behavior observed in the glassy state and also confirms the temperature dependence observed previously in the nonisothermal cold-crystallized sample.

Considering that high crystalline samples are being analyzed, the permanence of this β-process is a clear indication of its intramolecular nature as suggested previously for the other members of the series.[15]

Mobility after Nonisothermal Crystallization from Melt. Although with a very low intensity the β-process is the dominating process in this sample, the α-relaxation is still observed with very small magnitude. Interestingly, no α'-process was detected, and no further cold-crystallization was observed in the heating run.

The detected processes after each thermal treatment are summarized in Table 4.

Overall Behavior. In most of the semicrystalline samples investigated in this work, an additional process, α', emerges. The observation of a hindered process is usual in semicrystalline polymers. Williams,[16] Ezquerra et al.,[17] and Fukao and Miyamoto[34] report its existence for poly(ethylene terephthalate), in a condition where the material becomes 100% spherulitic but only 50% crystalline, the amorphous and crystalline regions being in intimate contact. The α'-process is thus attributed to motions of the constrained amorphous region within the spherulites and on their surfaces. Although not so frequent, the emergence of a new low frequency process is also reported for a few low molecular weight materials.[27,29] In the present case, EGDMA attains very high crystallinity degrees being unlikely that a bulk constrained amorphous part could exist within the crystallites; rather any amorphous fraction would be limited to surfaces on the crystals originating the detected α'-relaxation.

***β*- and *γ*-Traces in the Semicrystalline Materials.** In the samples crystallized nonisothermally (both coming from glassy and molten states), the temperature dependence of the β-relaxation seems to cross the α-process trace without merging (remember activation plots in Figures 4 and 9). This insensitivity of both α- and β-traces relative to each other is clearly seen in the melt-crystallized sample, where the faster α-relaxation

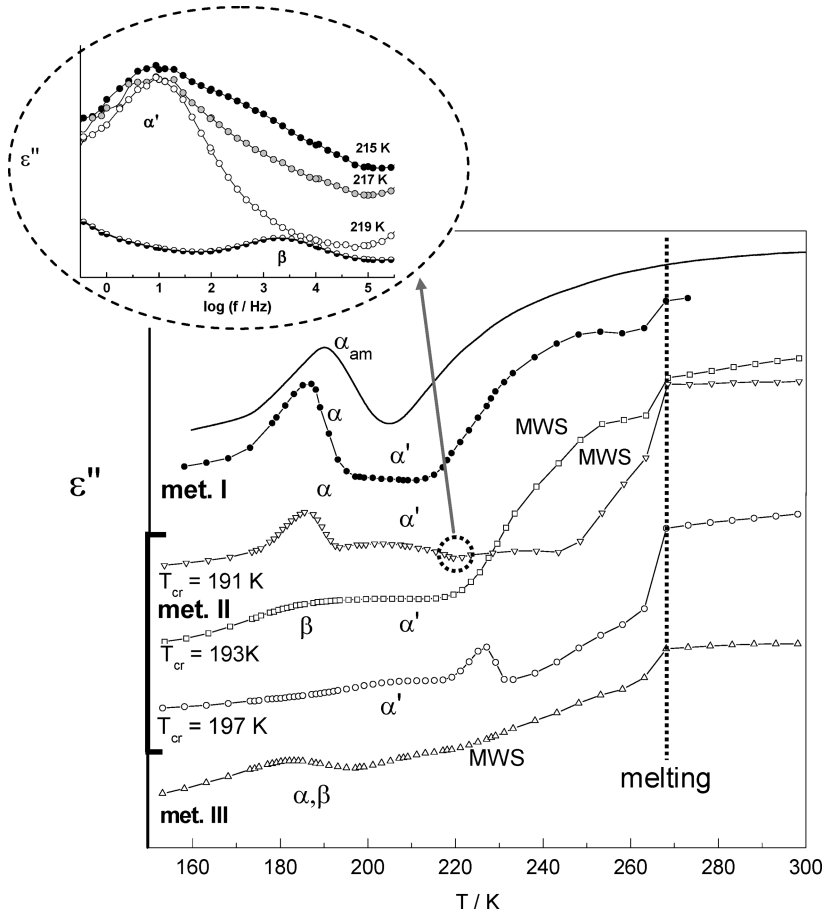

Figure 11. Isochronal dielectric loss at 100 Hz in logarithmic scale illustrating the dielectric behavior observed after different thermal treatments. The plots were displaced vertically to make the comparison easier. The magnitudes of the different processes should not be compared since distinct scales were used. Identification from top to bottom: solid line, cooling ramp from 298 to 153 K at 13 K·min^{-1} (stage 1 of method **I**) which led to the full amorphous solid; filled circles, subsequent heating (stage 2 of method **I**), where cold-crystallization occurred above ~183 K; T_{cr} = 197 K, T_{cr} = 193 K, and T_{cr} = 191 K, after isothermal cold-crystallization (method **II**) at the referred T_{cr}; met. **III**, after crystallization from melt. The isochronal plots were constructed taking data acquired isothermally after each thermal treatment, except for the data represented by the solid line. The inset shows some isotherms where the β-process continuously disappears originating the drop in the T_{cr} = 191 K trace (dashed circles), and its location is shown by the loss curve detected at 215 K in the specimen crystallized at 193 K (half-down circles). The vertical dashed line indicates the melting that occurs at the same temperature (263 K) for all samples.

crosses the slower β-process instead of merging into an $\alpha\beta$ or *a* process as found for a variety of materials (illustrated in Figure 10). This peculiar effect where the α- and β-traces cross without interfering with each other was also found by Lupaşcu et al. in atactic and syndiotactic polystyrene,[54] which was taken as an indication of independent dynamic processes. So, it can be assumed that the α- and β-processes detected in EGDMA evolve decoupled from each other.

As an alternative to this explanation, the observed behavior can also be rationalized conceiving that the remaining β-process is occurring in the semicrystalline material, in a different phase other than the bulklike amorphous fraction where the original α-relaxation takes place. This interpretation is not incompatible with the similarity observed for each conceivable β-process occurring in either amorphous bulklike or semicrystalline environments, which would follow the same trace in the activation plot since both relaxations can be originated by local dipolar fluctuations involving the same molecular unit.

In regard to the γ-trace detected after the sample being cold-crystallized at 193 K, it reveals a temperature dependence of relaxation times (Figure 9) that, in spite of some uncertainty, seems to agree with the linear behavior found in the glassy state. The insensitivity of the γ-relaxation time during conversion was already observed in other complex systems as partially polymerized mixtures[55] and for the members of the EGDMA series (n = 2, 3, and 4),[15,56] where τ_γ detected in the unreacted monomer remains unchanged upon polymerization.

Influence of Thermal History in the Crystallization Behavior of EGDMA. The evolving of crystallization is usually interpreted in terms of a nucleation/growth process, where crystallization requires the presence of a nucleus on which the crystals will subsequently grow.[57] For a variety of materials, the nucleation rate has a maximum above T_g, while the maximum growth rate is further displaced at higher temperatures somewhere between T_g and T_m.[2,58,59]

To gain a better understanding of the factors that determine crystallization of amorphous EGDMA and the possible location of those nucleation/growth mechanisms, we compare the results obtained subsequently to the distinct thermal pathways.

Figure 11 presents at 100 Hz the dielectric response (in logarithmic scale) after submitting EGDMA to the different thermal treatments tested in the present work.

The solid line in Figure 11 corresponds to the behavior found in the decreasing temperature run where crystallization was avoided being the clear signature of the α-process. Upon subsequent heating, cold-crystallization occurs slightly above 183 K (filled circles) suppressing the α-process. An identical behavior was undergone by a different sample previously cold-

crystallized for 2 h at 191 K (detailed analysis not reported here) where the α-process remained (triangles down) but disappeared under further heating. The α′- and β-relaxations seem to be the processes that persist after the nonisothermal crystallization of these two semicrystalline samples. Nevertheless, in the latter, an additional cold-crystallization occurred above 213 K as detected by the drop in ε'' (indicated by the circle in dashed line) extinguishing the β-process as shown in the isotherms included in the inset (the location of the β-process is undoubtedly indicated by the isotherm at 215 K of the sample crystallized at 193 K). This is the reason why data from a sample crystallized at 191 K were included since it is the only experiment where the β-process can be suppressed by supplementary crystallization.

In the sample melt-crystallized (up triangles) some contribution of the α-relaxation is still present, but no further crystallization occurs. In this kind of crystallization, coming from the molten state, nucleation and growth are rather simultaneous. Therefore, the absence of further crystallization (cold) could mean that in the melt-crystallized sample the mobility retained was not enough to promote further crystal grow in the subsequent heating run.

The isothermal crystallization at 197 K is the experiment where in only a single path neither α- nor β-processes are left. It seems that the greatest crystallization degree was attained for this sample.

In spite of the different crystallinities achieved and prethermal treatment, all the specimens melt at the same temperature, 263 K. It is interesting to point out that also the melting endotherms detected by DSC are independent of the thermal history (either after isothermal melt- and cold-crystallizations or after nonisothermal cold and melt-crystallizations): the respective endothermic peaks perfectly superpose (not shown). According to the Gibbs−Thomson equation,[60,61] this fact means that the crystals formed are large enough to make insignificant their surface free energy when compared with volume free energy, since the former is responsible for the dependence of melting temperature on the crystal size. Thus, DSC heating scans give no information about the dependence of crystal morphology with thermal history during crystallization. Nevertheless, a difference in the microstructure of the semicrystalline materials formed seems to be evident from dielectric results.

Conclusions

Ethylene glycol dimethacrylate is a low molecular weight glass former that can be obtained as a fully amorphous glass or in a nearly fully crystalline state depending on the thermal treatment to which it is subjected.

Molecular mobility of the amorphous material in the glassy state is characterized by two secondary relaxations, γ and β, attributed to local motions, which can be related to the corresponding relaxation processes in other *n*-EGDMA previously characterized. The cooperative α-relaxation is characterized by the common VFTH behavior with T_g, T_0, and fragility index values in line with those of their counterparts.

The α-relaxation is completely suppressed only when crystallization is preceded by cooling to a temperature below T_g. When the sample is melt-crystallized, the cooperative α-relaxation remains even strongly depleted.

On the other hand, the secondary β-relaxation when detected after crystallization becomes better resolved relative to the amorphous material. In spite of its significant depletion, it is observed in a broader temperature interval including that in which the α-relaxation was located in the amorphous material. The detection of β- and γ-processes after the vanishing of the cooperative α-relaxation means that its origin can be ascribed to molecular motions occurring in dimensions below the length-scale of cooperativity. Additionally, a low frequency α′-relaxation appears at advanced crystallization states, which can be due to mobility in amorphous regions adjacent to the crystal surfaces. The detection of this hindered process presents some similarity to what happens in semicrystalline polymers, but in the case of low molecular weight molecules, there appear interesting peculiarities that come from the differences in crystal morphology and the lack of connectivity in the crystal−amorphous interfaces between the molecules that remain in the amorphous fraction and those in the crystalline phase.

Interestingly enough is the insensitivity to conversion of the β-process location (and apparently of γ), reinforcing the previous assignment of secondary relaxations in the *n*-EGDMA series to very localized motions. This leads to a decoupling of their temperatures dependencies relative to that of the α-process which takes place in the amorphous bulk-like regions.

Dielectric relaxation proved to be sensible to the remaining mobility in a highly crystalline media.

Acknowledgment. The authors deeply acknowledge the helpful discussions with Prof. Graham Williams. Financial support to Fundação para a Ciência e Tecnologia (FCT, Portugal) is acknowledged through the project PTDC/CTM/64288/2006 and a postdoc grant SFRH/BPD/39691/2007 (M. T. Viciosa). J. L. Gómez Ribelles acknowledges the support of the Spanish Ministry of Science through project No. MAT2007-66759-C03-01 (including the FEDER financial support) and funding for research in the field of Regenerative Medicine through the collaboration agreement from the Conselleria de Sanidad (Generalitat Valenciana) and the Instituto de Salud Carlos III (Ministry of Science and Innovation).

References and Notes

(1) Carpentier, L.; Decressain, R.; Desprez, S.; Descamps, M. *J. Phys. Chem. B* **2006**, *110*, 457.
(2) Andronis, V.; Zografi, G. *J. Non-Cryst. Solids* **2000**, *271*, 236.
(3) Vallet-Regí, M.; Granado, S.; Arcos, D.; Gordo, M.; Cabaòas, M. V.; Ragel, C. V.; Salinas, A. J.; Doadrio, A. L.; San Román, J. *J. Biomed. Mater. Res.* **1998**, *39*, 423.
(4) Walstra, P. *Physical Chemistry of Food*; Marcel Dekker Inc.: New York, 2003; chap. XVI.
(5) Bhugra, C.; Rambhatla, S.; Bakri, A.; Duddu, S. P.; Miller, D. P.; Pikal, M. J.; Lechuga-Ballesteros, D. *J. Pharm. Sci.* **2007**, *96*, 1258.
(6) Seefeldt, K.; Miller, J.; Alvarez-Núñez, F.; Rodríguez-Hornedo, N. *J. Pharm. Sci.* **2007**, *96*, 1147.
(7) Hancock, B. C.; Shamblin, S. L.; Zografi, G. *Pharm. Res.* **1995**, *12*, 799.
(8) Yoshioka, M.; Hancock, B. C.; Zografi, G. *J. Pharm. Sci.* **1995**, *84*, 983.
(9) Dudognon, E.; Danède, F.; Descamps, M.; Correia, N. T. *Pharm. Res.* **2008**, *25*, 2853.
(10) Bland, M. H.; Peppas, N. A. *Biomaterials* **1996**, *17*, 1109.
(11) Krishnan, V. K.; Manjusha, K.; Yamuna, V. J. *Mater. Sci.-Mater. Med.* **1997**, *8*, 703.
(12) Alvarez-Lorenzo, C.; Hiratani, H.; Gómez-Amoza, J. L.; Martínez-Pacheco, R.; Souto, C.; Concheiro, A. *J. Pharm. Sci.* **2002**, *91*, 2182.
(13) Chetoni, P.; Di Colo, G.; Grandi, M.; Morelli, M.; Saettone, M. F.; Darougar, S. *Eur. J. Pharm. Biopharm.* **1998**, *46*, 125.
(14) Viciosa, M. T.; Dionísio, M. *J. Non-Cryst. Solids* **2004**, *341*, 60.
(15) Viciosa, M. T.; Brás, A. R.; Gómez Ribelles, J. L.; Dionísio, M. *Eur. Polym. J.* **2008**, *44*, 155.
(16) Williams, G. *Adv. Polym. Sci.* **1979**, *33*, 59.
(17) Ezquerra, T. A.; Baltá-Calleja, F. J.; Zachmann, H. G. *Polymer* **1994**, *35*, 2600.
(18) Dionísio, M.; Viciosa, M. T.; Wang, Y.; Mano, J. F. *Macromol. Rapid Commun.* **2005**, *26*, 1423.
(19) Brás, A. R.; Viciosa, M. T.; Wang, Y.; Dionísio, M.; Mano, J. F. *Macromolecules* **2006**, *39*, 6513.
(20) Mijoviæ, J.; Sy, J. W. *Macromolecules* **2002**, *35*, 6370.

(21) Fitz, B. D.; Andjelić, S. *Polymer* **2003**, *44*, 3031.
(22) Kanchanasopa, M.; Runt, J. *Macromolecules* **2004**, *37*, 863.
(23) Laredo, E.; Graimau, M.; Barriola, P.; Bello, A.; Müller, A. J. *Polymer* **2005**, *46*, 6532.
(24) Soccio, M.; Nogales, A.; Lotti, N.; Munari, A.; Ezquerra, T. A. *Polymer* **2007**, *48*, 4742.
(25) Sanz, A.; Nogales, A.; Ezquerra, T. A.; Lotti, N.; Munari, A.; Funari, S. S. *Polymer* **2006**, *47*, 1281.
(26) Massalska-Arodz, M.; Williams, G.; Smith, I. K.; Conolly, C.; Aldridge, G. A.; Dabrowski, R. *J. Chem. Soc., Faraday Trans.* **1998**, *94*, 387.
(27) Dobbertin, J.; Hannemann, J.; Schick, C.; Potter, M.; Dehne, H. *J. Chem. Phys.* **1998**, *108*, 9062.
(28) Massalska-Arodz, M.; Williams, G.; Thomas, D. K.; Jones, W. J.; Dabrowski, R. *J. Phys. Chem. B* **1998**, *103*, 4197.
(29) Minoguchi, A.; Nozaki, R. *J. Non-Cryst. Solids* **2002**, *307*−*310*, 246.
(30) Hédoux, A.; Denicourt, T.; Guinet, Y.; Carpentier, L.; Descamps, M. *Solid State Commun.* **2002**, *122*, 373.
(31) Jiménez-Ruiz, M.; Ezquerra, T. A.; Sics, I.; Fernández-Díaz, M. T. *Appl. Phys. A* **2002**, *74*, S543.
(32) Rengarajan, G. T.; Beiner, M. *Lett. Drug Des. Discovery* **2006**, *3*, 723.
(33) Alie, J.; Menegotto, J.; Cardon, P.; Duplaa, H.; Caron, A.; Lacabanne, C.; Bauer, M. *J. Pharm. Sci.* **2004**, *93*, 218.
(34) Fukao, K.; Miyamoto, Y. J. *J. Non-Cryst. Solids* **1997**, *212*, 208. Fukao, K.; Miyamoto, Y. J. *J. Non-Cryst. Solids* **1998**, *235*−*237*, 534.
(35) Alves, N. M.; Mano, J. F.; Balaguer, E.; Meseguer Dueñas, J. M.; Gómez Ribelles, J. L. *Polymer* **2002**, *43*, 4111.
(36) Shafee, E. El. *Eur. Polym. J.* **2001**, *37*, 1677.
(37) Wang, Y.; Gómez Ribelles, J. L.; Salmerón Sánchez, M.; Mano, J. F. *Macromolecules* **2005**, *38*, 4712.
(38) Viciosa, M. T.; Correia, N. T.; Salmerón Sánchez, M.; Carvalho, A. L., Romão, M. J.; Gómez Ribelles, J. L.; Dionísio, M. *J. Phys. Chem. B*, DOI: 10.1021/jp903212g.
(39) Affouard, F., *Private communication*. The estimation of the dipolar moment was accomplished by using Gaussian98 [Frisch, M. J. *Gaussian 98*, Revision A.11.1; Gaussian, Inc.: Pittsburgh PA, 2001]. Base: B3LYP/6-31G*.
(40) Havriliak, S.; Negami, S. *Polymer* **1967**, *8*, 161. Havriliak, S.; Negami, S. *J. Polym. Sci. C* **1966**, *16*, 99.
(41) Schönhals, A.; Kremer, F. Analysis of Dielectric Spectra. In *Broadband Dielectric Spectroscopy*; Kremer, F., Schönhals, A., Eds.; Springer Verlag: Berlin, 2003; Chapter 3.
(42) Boersema, A.; van Turnhout, J.; Wübbenhorst, M. *Macromolecules* **1998**, *31*, 7453.
(43) Schröter, K.; Unger, R.; Reissig, S.; Garwe, F.; Kahle, S.; Beiner, M.; Donth, E. *Macromolecules* **1998**, *31*, 8966.
(44) Fröhlich, H. *Theory of Dielectrics*; Oxford Univ. Press, 1958.
(45) Wunderlich, B. *J. Chem. Phys.* **1958**, *29*, 1395.
(46) Diogo, H. P.; Moura Ramos, J. J. *J. Chem. Educ.* **2006**, *83*, 1389.
(47) Vogel, H. *Phys. Zeit.* **1921**, *22*, 645.
(48) Fulcher, G. S. *J. Am. Ceram. Soc.* **1925**, *8*, 339.
(49) Tammann, G.; Hesse, W. *Z. Anorg. Allg. Chem.* **1926**, *156*, 245.
(50) Richert, R.; Blumen, A. Eds. *Disorder Effects on Relaxational Processes*; Springer: Berlin, 1994.
(51) Böhmer, R.; Ngai, K. L.; Angell, C. A.; Plazek, D. J. *J. Chem. Phys.* **1993**, *99*, 4201.
(52) Angell, C. A. *J. Non-Cryst. Solids* **1991**, *131*−*133*, 13. Angell, C. A. *J. Res. Natl. Inst. Stand. Technol.* **1997**, *102*, 171.
(53) Qin, Q.; McKenna, G. B. *J. Non-Cryst. Solids* **2006**, *352*, 2977.
(54) Lupa°cu, V.; Picken, S. J.; Wübbenhorst, M. *Macromolecules* **2006**, *39*, 5152.
(55) Beiner, M.; Ngai, K. L. *Macromolecules* **2005**, *38*, 7033.
(56) Viciosa, M. T.; Rodrigues, C. M.; Dionísio, M. *J. Non-Cryst. Solids* **2005**, *351*, 14. In this reference, the actual γ-process found in *n*-ethylene glycol dimethacrylates was designated as β since only one secondary relaxation was detected.
(57) Shelby, J. E. *Introduction to Glassy Science and Applications*; Royal Society of Chemistry: Cambridge, United Kingdom, 2002.
(58) Rao, C. N. R.; Rao, K. J. *Phase Transitions in Solids*; McGraw-Hill: New York, 1978.
(59) Owen, A. E. *Amorphous Solids and the Liquid State*; Plenum: New York, 1985.
(60) Wunderlich, B. *Macromolecular Physics*; Academic Press: London, 1980; Vol. 3.
(61) Zhou, H.; Wilkes, G. L. *Polymer* **1997**, *38*, 5735.

JP903208K